Soft Matter

RSC Publishing

PAPER

View Article Online
View Journal | View Issue

Cite this: *Soft Matter*, 2013, **9**, 7145

How deprotonation changes molecular self-assembly – an AFM study in liquid environment

Martin Schreiber, Michael Eckardt, Stefanie Klassen, Holger Adam, Martin Nalbach, Lukas Greifenstein, Felix Kling, Markus Kittelmann, Ralf Bechstein and Angelika Kühnle*

We study the influence of Alizarin Red S deprotonation on molecular self-assembly at the solid–liquid interface of the natural cleavage plane of calcite immersed in aqueous solution. To elucidate the adsorption details, we perform pH dependent high-resolution atomic force microscopy measurements. When Alizarin Red S is deposited onto calcite(10.4) in a liquid environment at an acidic pH of 5, weakly bound, ordered islands with a (3 × 3) superstructure are observed. A sharp structural transition is revealed when increasing the pH above 8. Above this pH, stable needle-like structures oriented along the [01.0] direction form on the surface. Comparing these results with potentiometric titration data allows for unambiguously assigning the two molecular structures to the single and two-fold deprotonated moieties of Alizarin Red S. Our work, thus, illustrates the decisive impact of the protonation state on molecular self-assembly.

Received 24th January 2013
Accepted 17th May 2013

DOI: 10.1039/c3sm50262g

www.rsc.org/softmatter

Introduction

Self-assembly of organic molecules constitutes a powerful strategy for creating functional materials with tailor-made properties.[1] Consequently, molecular self-assembly on surfaces has been studied intensively for fabricating functional molecular devices on surfaces.[2,3] So far, most of the work based on high-resolution imaging has been carried out in the well-defined environment of ultra-high vacuum (UHV). The UHV-based approach offers the advantage of a straightforward data interpretation and easy comparison with theoretical work. Future applications, however, will require the knowledge of molecular structure formation under realistic, *i.e.*, ambient or liquid conditions. In this case, the presence of water and airborne molecules can significantly alter the delicate balance of intermolecular and molecule–surface interactions that govern the resulting molecular structure at the surface. For molecules that can deprotonate in solution, the pH is an important parameter that can be exploited for tuning the molecule–surface interaction.

Here, we present a molecule adsorption study in an application-oriented, liquid environment. Due to recent progress in atomic force microscopy,[4–6] it is nowadays possible to image the solid–liquid interface in direct space with molecular-scale resolution. High-resolution atomic force microscopy (AFM) images taken at the solid–liquid interface at various pH values offer unprecedented insights into the binding configuration of the organic molecule at the surface as a function of the molecular protonation state.

In this study, we investigate the adsorption of 3,4-dihydroxy-2-anthraquinonesulfonic acid sodium salt (Fig. 1a), commonly

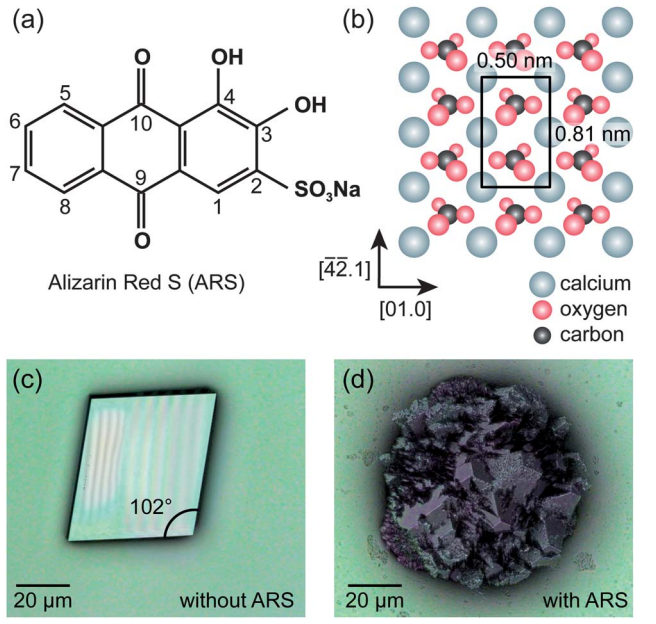

Fig. 1 Molecule and substrate investigated in this study. (a) Alizarin Red S (ARS). (b) Calcite cleavage plane, $CaCO_3$(10.4). The surface unit cell is marked by a rectangle. Calcite crystallites grown using the ammonia-diffusion method, (c) from pure solution and (d) from a solution containing ARS.

Johannes Gutenberg University Mainz, Institute of Physical Chemistry, Duesbergweg 10-14, 55099 Mainz, Germany. E-mail: kuehnle@uni-mainz.de; Fax: +49 6131 39 53930; Tel: +49 6131 39 23930

known as Alizarin Red S (ARS), onto the (10.4) cleavage plane of calcite (Fig. 1b), the most stable modification of calcium carbonate, $CaCO_3$. ARS is a widely used dye[7] that finds applications in, *e.g.*, histology for staining bones[8,9] as well as geology for differing and separation (flotation) between calcite and other calcium-containing rocks.[10,11] In these and other applications, the adsorption of ARS onto the surface and especially the interaction with the calcium ions are the key aspects for understanding the mode of action.[12,13] ARS is known to form complexes with Ca^{2+} ions in solution but also at the calcite surface.[14,15] The interaction between ARS and calcite is evident from $CaCO_3$ crystallization experiments in the absence and presence of ARS as shown in Fig. 1(c and d).[16] In the absence of ARS, single-crystalline rhombohedra form, which can be unambiguously identified as calcite (Fig. 1c). In contrast, in the presence of ARS distorted polycrystalline material grows (Fig. 1d).

We study the adsorption of ARS onto calcite(10.4) using frequency modulation (FM) AFM under liquid conditions.[17] Images taken in the acidic range reveal island structures. A transition to needle-like structures is found at a pH around 8, which coincides with a buffer plateau in the titration curves. Consequently, we attribute the structural change to a change in the deprotonation state, elucidating the influence of the deprotonation state on the structure formation. Our work, thus, demonstrates the decisive influence of the protonation state on molecular self-assembly.

Materials and methods

ARS

ARS (*p.a.* quality) was purchased from Merck KGaA (Germany) and used without further purification. Potentiometric titration experiments were carried out using a Metrohm 702 SM Titrino instrument equipped with a Metrohm pH glass electrode (No. 6.0256.100, Metrohm, Switzerland). Standard solutions of $CaCl_2$ (0.5 M) and NaOH (0.1 M) were obtained from Sigma Aldrich, Germany. Standard solution of HCl (1 M) was purchased from Carl Roth, Germany. We titrated 20 ml of solutions containing no or 0.06 mmol ARS and no or 0.04 mmol $CaCl_2$ with 0.1 mM NaOH. The ionic strength was kept constant by adding 2 mmol NaCl. An amount of 0.1 mmol HCl was added to better resolve the first deprotonation step.

The concentration of calcium ions was quantified by measuring the Ca^{2+}activity with a pH meter (872 pH lab and electrode No. 6.0256.100, Metrohm, Switzerland) and a calcium selective electrode (No. 6.0508.110, Metrohm). The calcium electrode was calibrated with calcium chloride solutions of known concentrations, ranging from 0.05 mM to 15 mM. The calibration was performed in the presence of HCl and NaCl to guarantee a constant pH and ionic strength, respectively. The pH was monitored with a Schott laboratory pH meter (CG 842) equipped with a BlueLine electrode from Schott (Germany). To study the complex formation of ARS with calcium ions, a 0.1 M ARS solution was added in increments of 50 μl to 100 ml of an aqueous 0.5 mM $CaCl_2$ solution.

Crystallization experiments were done using the standard ammonia-diffusion method.[18] Calcite crystallites were grown from $CaCl_2$ solution with and without ARS additive and crushed ammonium carbonate at the bottom of the desiccator. The resulting crystals were examined with a laser scanning microscope (Keyence VK-8710, Japan).

FM AFM in liquids

Liquid AFM experiments were carried out with a modified AFM instrument that has been optimized for frequency modulation imaging at the solid–liquid interface.[17] All images were taken with a closed liquid cell (Bruker Nano Surfaces Division, USA). For each experiment, a freshly cleaved calcite crystal (Korth Kristalle GmbH, Germany) was inserted into the cell and equilibrated with the solution containing the molecules. All experiments were performed in a saturated $CaCO_3$ solution to prevent dissolution of the calcite sample. The pH was adjusted by adding 0.1 M NaOH solution. As force sensors, we used gold-coated, p-doped silicon cantilevers (PPP-NCHAuD, Nanosensors, Switzerland) with a resonance frequency of about 160 kHz, a spring constant of about 40 N m^{-1}, and a Q value of around 8 in Milli-Q water (Millipore GmbH, Germany). The cantilever oscillation amplitude was kept constant at values between 1 nm and 20 nm.

Results and discussion

Deprotonation of ARS and complex formation with calcium

The ARS molecule contains two hydroxyls (Fig. 1a) which may donate one proton each. Reported pK_a values for ARS are 5.8 for the hydroxyl in position 3 and above 11 for the hydroxyl in position 4.[19–22] Potentiometric titration of an ARS solution containing 0.06 mmol ARS (Fig. 2a, triangles) gives about the same value ($pK_a = 5.9$) for the first hydroxyl. The second pK_a is not straightforwardly accessible with this method but is clearly above pH 11. When adding 0.04 mmol $CaCl_2$ to the same ARS solution (Fig. 2a, open circles), two new buffer levels establish at $pK_1 = 4.3$ and $pK_2 = 8.1$. As sodium and chlorine ions are present in all solutions, the only difference in the latter case is the presence of calcium ions. From this comparison, we can conclude that ARS deprotonates much easier, *i.e.*, at lower pH in the presence of calcium ions. This can be explained by complex formation of ARS with calcium cations.[14,15]

To study the complex formation of ARS with calcium ions, we titrated an aqueous $CaCl_2$ solution, which was acidified with HCl, with ARS (Fig. 2b). Apparently, already at an acidic pH as low as 2.9 the Ca^{2+} concentration decreases substantially when ARS is added. This finding shows that the Ca–ARS complex forms already when ARS is still fully protonated. It is reasonable to assume that the strength of the complex increases when ARS deprotonates. This serves as an explanation as to why ARS deprotonation is facilitated in the case of complex formation with calcium. Therefore, we assign the two buffer regions in Fig. 2a (open circles) to the deprotonation of the Ca–ARS complex. The values pK_1 and pK_2 thus correspond to the deprotonation of the hydroxyls in positions 3 and 4 of the Ca–ARS complex, respectively.

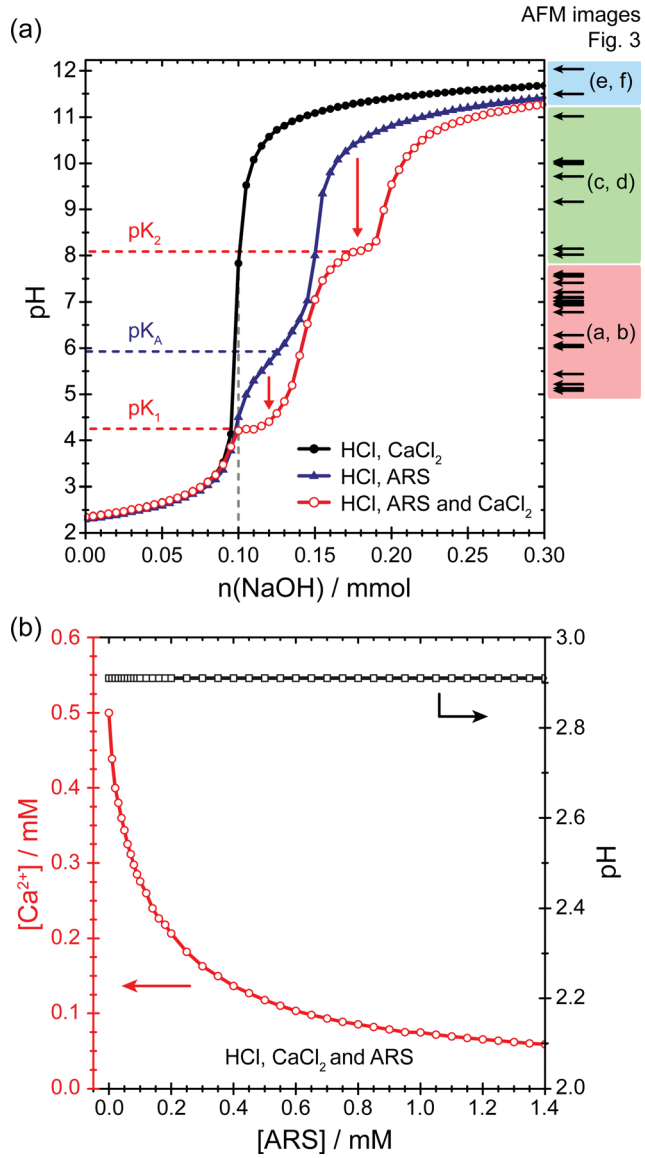

Fig. 2 (a) Titration curves of reference solution without ARS (discs), ARS solution (triangles) and ARS solution with Ca^{2+} ions (open circles). Dashed lines mark the neutralization of HCl and the buffer plateaus. The pH levels of the AFM experiments are indicated and the colour code refers to representative images (Fig. 3). (b) Titration of a $CaCl_2$ solution with ARS at a constant pH showing decrease in the Ca^{2+} ion concentration upon ARS addition, in agreement with a complex formation of ARS with calcium ions.

In saturated calcium carbonate solution, as used for the AFM experiments, titration yields the same buffer plateaus as in $CaCl_2$ solution (not shown). Hence, we can precisely control the protonation state of ARS in our AFM experiments by adjusting the pH of the calcium carbonate solution.

Molecular structure of ARS on calcite(10.4) in saturated $CaCO_3$ solution

To elucidate the influence of deprotonation on molecular self-assembly, we investigated the molecular structures of ARS on calcite(10.4) in a liquid environment as a function of the pH value. The AFM experiments cover the entire accessible pH range from pH 5 to pH 12 (compare arrows to the right in Fig. 2a). Below pH 5, the calcite sample is etched and above pH 11, the saturation concentration of the $CaCO_3$ solution decreases rapidly leading to precipitation. Representative AFM images are shown in Fig. 3.

At an acidic pH of 5 up to pH 8, we observe molecular island formation (Fig. 3a and b). The monolayer islands have an apparent height of approximately 1.3 nm and reveal a (3×3) superstructure.

When increasing the pH, a significantly different structure is observed (Fig. 3c and d). From pH around 8 up to pH 11 needle-like structures are present on the calcite surface and the molecular islands have vanished entirely. The needles have an apparent height of around 0.7 nm and are aligned along the [01.0] direction. High-resolution images (Fig. 3d) reveal a periodic structure in the [01.0] direction with a repeat distance of 1.5 nm, which is consistent with a $(3 \times n)$ superstructure.

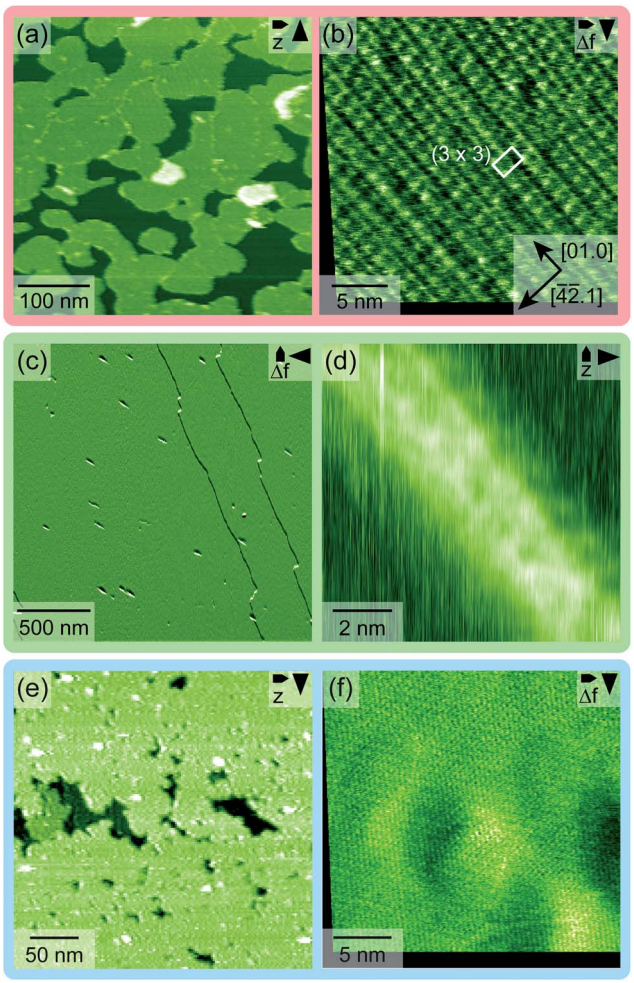

Fig. 3 FM AFM images of calcite(10.4) in saturated $CaCO_3$ solution containing ARS at various pH levels. At pH values between 5 and 7.6 molecular islands form (a and b); between pH 8 and 11 needle-like ad-structures are present (c and d); above pH 11 precipitation can be seen (e and f). Topography (z) and detuning images (Δf) are corrected for thermal drift (Fig. 3b and f).

Upon further increasing the pH above 11, $CaCO_3$ precipitation is visible during AFM data acquisition with layer-by-layer growth of the calcite. In the presence of ARS, this leads to a somewhat unusual appearance of the surface (Fig. 3e). The calcite surface is not flat, but several incomplete layers are visible, indicating distorted growth. Despite this distorted growth, an atomically flat calcite(10.4) surface can be identified in high-resolution images (Fig. 3f), confirming the assignment of calcite growth.

The molecular islands revealed at low pH are easily destroyed when scanning at large tip–sample interaction indicating a weak molecule–surface interaction. Whenever an island was removed, a new island formed shortly after decreasing the tip–sample interaction. In sharp contrast to the molecular islands, the needle-like structures remained stable on the surface also at high tip–sample interaction and it was not possible to deliberately destroy a needle without losing the imaging capability of the tip. This finding indicates a much stronger molecule–surface interaction in the case of the needle-like structures.

To interpret the findings obtained with FM AFM, we have to consider the protonation state of ARS in dependence on the pH of the solution. ARS possesses two hydroxyl groups in positions 3 and 4. The first hydroxyl group (position 3) is associated with a pK_a value of 5.9 in the absence of calcium ions. When ARS forms a complex with the Ca^{2+} ions present in solution, this value is lowered to around $pK_1 = 4.3$, see Fig. 2a (open circles). A similar effect can be anticipated for ARS forming a complex with the Ca^{2+} ions in the calcite surface. This is confirmed by the fact that the same molecular islands are observed for pH values above and below the pK_a of 5.9. Thus, for images taken at a pH around 5 and higher, we expect the hydroxyl group at position 3 to be deprotonated. Upon increasing the pH above the second buffer regime at pK_2, a structural change is observed. This indicates that the second hydroxyl group (position 4) deprotonates from ARS bound to the calcite surface in a similar way as from a Ca–ARS complex in solution.

From this comparison of AFM images at different pH with the titration experiments we can summarize that the molecules forming the islands are deprotonated at the hydroxyl group in position 3. In this state, the molecule can bind towards the calcium cation of the surface *via* the 3-C–O^- group and towards the protruding oxygen atom of the surface *via* the 4-C–OH group. The needle structure, however, is formed by fully deprotonated ARS molecules. That is evidently clear from the fact that it is exactly the pH region around pK_2 (Fig. 2a) where the islands disappear and the needles appear. In this configuration, ARS can bind to the surface in a much more stable form with both C–O^- groups anchoring towards a surface calcium cation. The strengthening of the Ca–ARS complex upon deprotonation is directly observed in our AFM experiments since we find the needles more strongly bound as compared to the molecular islands.

Upon further increasing the pH, $CaCO_3$ precipitation sets in, resulting in calcite growth. We speculate that firmly bound ARS molecules are responsible for the distorted growth of the calcite sample for pH above 11 similar to what we observed in our crystallization experiments (Fig. 1d). Moreover, at a pH above 11, calcium hydroxide is known to form at the surface, which might replace the needles.[23] These two effects might explain why the needle-like structures are no longer visible when increasing the pH to very high values.

Summary and conclusions

In conclusion, the pH-dependent adsorption study of ARS onto calcite(10.4) under liquid conditions elucidates molecular-scale details of the binding configuration, governing the subtle interaction interplay that steers molecular self-assembly. When ARS is deposited under liquid conditions, the pH needs to be considered as the protonation state of the molecule significantly influences the binding towards the surface. At low pH, only one hydroxyl group is deprotonated, resulting in a possible adsorption configuration mediated by the 3-C–O^- and the 4-C–OH groups. The islands that form in this case are characterized by a weak binding towards the surface.

When increasing the pH above 8, both hydroxyl groups are deprotonated. In this state, the molecules bind towards the surface with two C–O^- groups, which allows for forming firmly anchored, needle-like structures.

By comparing the molecular structure formation at various pH values, our work elucidates the significant impact of molecule deprotonation on molecular self-assembly.

Acknowledgements

The authors are grateful to Michèle Grüner, Erik Kersten and Julia Neff for useful comments and support during data collection. We thank the group of Wolfgang Tremel for stimulating discussions and generous access to the titration equipment.

Notes and references

1 J. M. Lehn, *Angew. Chem., Int. Ed. Engl.*, 1988, **27**, 89.
2 J. V. Barth, *Annu. Rev. Phys. Chem.*, 2007, **58**, 375.
3 A. Kühnle, *Curr. Opin. Colloid Interface Sci.*, 2009, **14**, 157.
4 T. Ando, T. Uchihashi and T. Fukuma, *Prog. Surf. Sci.*, 2008, **83**, 337.
5 S. Rode, N. Oyabu, K. Kobayashi, H. Yamada and A. Kühnle, *Langmuir*, 2009, **25**, 2850.
6 T. Fukuma, M. Kimura, K. Kobayashi, K. Matsushige and H. Yamada, *Rev. Sci. Instrum.*, 2005, **76**, 053704.
7 C.-H. Wunderlich and G. Bergerhoff, *Chem. Ber.*, 1994, **127**, 1185.
8 H. Puchtler, S. N. Meloan and M. S. Terry, *J. Histochem. Cytochem.*, 1969, **17**, 110.
9 C. J. S. Ibsen and H. Birkedal, *Nanoscale*, 2010, **2**, 2478.
10 G. M. Friedman, Identification of Carbonate Minerals by Staining Methods, *J. Sediment. Petrol.*, 1959, **29**, 87.
11 H. Baldauf and H. Schubert, in *Correlations between Structure and Adsorption for Organic Depressants in Flotation*, AIME, 1980, p. 767.
12 D. N. Misra, *Colloids Surf.*, 1992, **66**, 181.

13 T. Moriguchi, K. Yano, S. Nakagawa and F. Kaji, *J. Colloid Interface Sci.*, 2003, **260**, 19.
14 P. Virtanen and K. Isotupa, *Acta Anat.*, 1980, **108**, 202.
15 L. Wu and W. Forsling, *Acta Chem. Scand.*, 1992, **46**, 418.
16 V. Kohlschütter and C. Egg, *Helv. Chim. Acta*, 1925, **8**, 697.
17 S. Rode, R. Stark, J. Lübbe, L. Tröger, J. Schütte, K. Umeda, K. Kobayashi, H. Yamada and A. Kühnle, *Rev. Sci. Instrum.*, 2011, **82**, 073703.
18 J. Ihli, P. Bots, A. Kulak, L. G. Benning and F. C. Meldrum, *Adv. Funct. Mater.*, 2013, **23**, 1965.
19 A. Holmgren, L. Wu and W. Forsling, *Spectrochim. Acta, Part A*, 1999, **55**, 1721.
20 V. M. Ivanov, E. M. Adamova and V. N. Figurovskaya, *J. Anal. Chem.*, 2010, **65**, 473.
21 A. Turcanu and T. Bechtold, *Dyes Pigm.*, 2011, **91**, 324.
22 H. E. Zittel and T. M. Florence, *Anal. Chem.*, 1967, **39**, 320.
23 D. Gebauer, A. Völkel and H. Cölfen, *Science*, 2008, **322**, 1819.